2009

ELECTRIC FLOW ACROSS A CIRCULAR SPOT BETWEEN PARALLEL PLATES

Reza Haj Mohammad Jafar

ELECTRIC FLOW ACROSS A CIRCULAR SPOT BETWEEN PARALLEL PLATES

by

Reza Haj Mohammad Jafar

Graduate Program in Engineering Science
Department of Mechanical and Materials Engineering

Submitted in partial fulfillment
of the requirements for the degree of
Master of Engineering Science

School of Graduate and Postdoctoral Studies
The University of Western Ontario
London, Ontario, Canada

Abstract

A mathematical treatment of the general problem of electrical contacts and heating related to MEMS switch contacts is developed. The spatial distribution of the potential, the current and the temperature in a special case of electrical contact between two gold bodies whose thermal and electrical conductivities vary with temperature is analyzed, and an explanation for the collapse of gold contact system before reaching the melting point is given. For this purpose three different methods are applied. First, we develop an exact solution, which involves with solving a dual integral equation leading to a Fredholm integral equation, that is solved numerically. Secondly, a simple model to obtain an approximate resistance of an a-spot system is presented. Finally, another approximate solution is developed, where the variational method is implemented to reduce the complicated computations of the exact method. Excellent agreement is demonstrated between the results of the exact and the variational methods for all sizes of a-spots in contact systems.

Acknowledgements

I sincerely appreciate the invaluable guidance, consistent encouragement and great assistance of my advisor, Professor John Dryden. Without his support, the completion of this work would be impossible. I would like to express many thanks to my colleague, Mohsen Mohammadi for his assistance and generous help, during the course of this work. I also owe special thanks to my family and friends, whose continuous moral support made this thesis possible.

Contents

List of Figures

Nomenclature

L	sample length
r, a	the real contact radius of an a-spot
A	the real contact area of an a-spot
k	thermal conductivity
k_0	thermal conductivity at room temperature
T	absolute temperature
T_0	room temperature
V	potential
S	surface
V_0	applied voltage
I	current
j	current density
V_0^*	dimensionless voltage
I^*	dimensionless current
R	Resistance
α	the temperature coefficient of electrical resistivity
β	the temperature coefficient of thermal conductivity
ρ	electrical resistivity
ρ_0	electrical resistivity at room temperature
σ	electrical conductivity
σ_0	electrical conductivity at room temperature
θ	super-temperature, $\theta = T - T_0$
θ_m	maximum super-temperature
θ_m^*	dimensionless maximum super-temperature

Chapter 1

Introduction

In view of the increasing number of Micro-Electro-Mechanical systems (MEMS) involving surface contact, an understanding of the behaviour of MEMS contact interfaces is imperative. Touch-mode MEMS devices are advantageous in many applications, such as electrostatic actuators, microswitches, and microrelays. The performance and lifetime of such microdevices depend on the behaviour of their contact surfaces [1].

A Micro-Electro-Mechanical system (MEMS) is a batch-fabricated (microfabricated) system that contains both electrical and mechanical components with characteristics sizes ranging from nanometers to millimeters. Initially MEMS techniques were borrowed directly from integrated circuit (IC) fabrication technologies. A few of advantages include very low cost contributed to batch fabrication, tremendous size, weight and power reduction, and simultaneous great performance improvement [2, 3].

The development and application of MEMS and NEMS (Nano-Electro-Mechanical System) are critical to the current world as they will lead to major breakthrough in information technology, computers, medicine, health, manu-

facturing, transportation, energy, avionics, security, etc. Nowadays developing tendencies in engineering science have increased the importance on integrated synthesis, analysis, design and control of advanced MEMS and NEMS [4].

MEMS applications and markets begin where traditional IC applications and markets end. Commercially successful devices and systems that apply MEM technologies include many micro- or nano-scale sensors (e.g., inertial sensors, pressure sensors, chemical sensors, etc.), actuators (e.g., micro-mirrors, micro-relays, micro-valves, etc.), and other Microsystems [2]. Today, MEMS are mostly found in automotive industry, but the devices have already extended to biomedical, computer, wireless and optical communication systems, military and other industrial areas.

With the recent progress of MEMS technology, the development of MEMS devices for radio frequency (RF) applications has been growing rapidly. RF MEMS devices have a broad range of potential applications in wireless communication, space, military, instrumentation, etc. RF MEMS switches are one of the most promising surface-micro-machined devices that have attracted many research efforts in recent years. Compared with conventional switches such as PIN diode or FET switches, RF MEMS switches show many advantages in terms of near-zero power consumption, very high isolation and linearity, low insertion loss, etc [5, 6]. Also, RF MEMS switches can be applied in broad areas because of their frequencies from RF to millimetre-wave (0.1 to 100 GHz), such as Radar Systems for Defence Applications (5-94 GHz), Automotive Radars: 24, 60, and 77 GHz, Satellite Commucation Systems (12-35 GHz), and wireless Communication Systems (0.8-6 GHz) [6].

For their actuation mechanism RF MEMS switches can be divided into electrostatic, magnetic, thermal, and piezoelectric types. Currently most of researches focus on electrostatic types because of its spectacular RF performance

[6]. From their contact mechanisms two types of RF MEMS switches can be divided: metal contacting and capacitive coupling. MEMS metal contacting switches has broader frequency coverage than capacitive coupling switches which are not suitable for low frequency applications because of the capacitance nature. However, the contact lifetime of capacitive coupling switches is obviously longer than of the metal contacting switches [3]. In addition, RF MEMS switches can be catalogued into series and shunt switches in terms of applications. Most metal contacting switches are often used as serial switches while the capacitive coupling switches are used for shunt switches. In this thesis we mainly focus on a metal contacting RF MEMS switch.

Even though RF MEMS switches have many advantages over traditional switches, there are still some problems need to be solved in the future, such as relatively low speed and power handling (lower than 100mW), high-voltage drive (reliable operation at 20-80V), reliability (lower than 10 billions cycle), packaging, cost, and etc. [6].

Currently, the main failure analysis issue for RF MEMS metal contacting switches focuses on contact metallurgy. Some of the failure mechanisms include adhesion, thermal softening, melting, micro-welding, material transfer, and increased contact resistance, etc. [7, 8, 9]. In addition, the surface interaction due to deformation, current flow, heat generation affect the failure mechanisms significantly.

1.1 Temperature-voltage relation

All metal surfaces are rough on microscale although they are prepared carefully. The nature of the contact between two metals is markedly influenced by

the roughness of the two contact surfaces. When two metals are bought into contact, only highest asperities of the surfaces would have mechanical contact. The true contact area is just a small fraction of the nominal contact area (10^{-4} to 10^{-2}) [10].

Upon passage of an electrical current through the contacting metals, the current flow must pass the contact area through the highest asperities. The electrical current lines converge when approaching to the contact interface and then diverge. The constriction resistance causes the Joule heating in the contact region, therefore the temperature in the contact patch is much higher than the surrounding bulk metal [10, 11, 12]. The heat generation in the contact interface may cause thermal softening, melting, micro-welding, etc., decreasing the reliability and life of devices. Figure 1.1 shows the molten gold has splashed from micro-contact interfaces onto the surrounding cold metal, where it has frozen.

The conventional method to determine the temperature of electrically heated contacts is based on using the theoretical temperature-voltage relation [10, 13], which indicates the relation between the applied voltage across the contact and maximum temperature in the contact interface. By utilizing this relation, we can calculate the maximum temperature in contact interface from the applied contact voltage. Because this relationship involves only with material properties (electrical and thermal conductivities), it is true for electrical contacts of any shape and dimensions. Further, Greenwood developed a mathematical treatment of the general problem of electrically heated bodies [11, 13]. The researchers in [11] studied a contact system between two gold solids and investigated the contact temperature and heat generated in the constricted region due to the passage of an electric current from a high impedance source. They observed the collapse of the contact system occurred at the temperature of

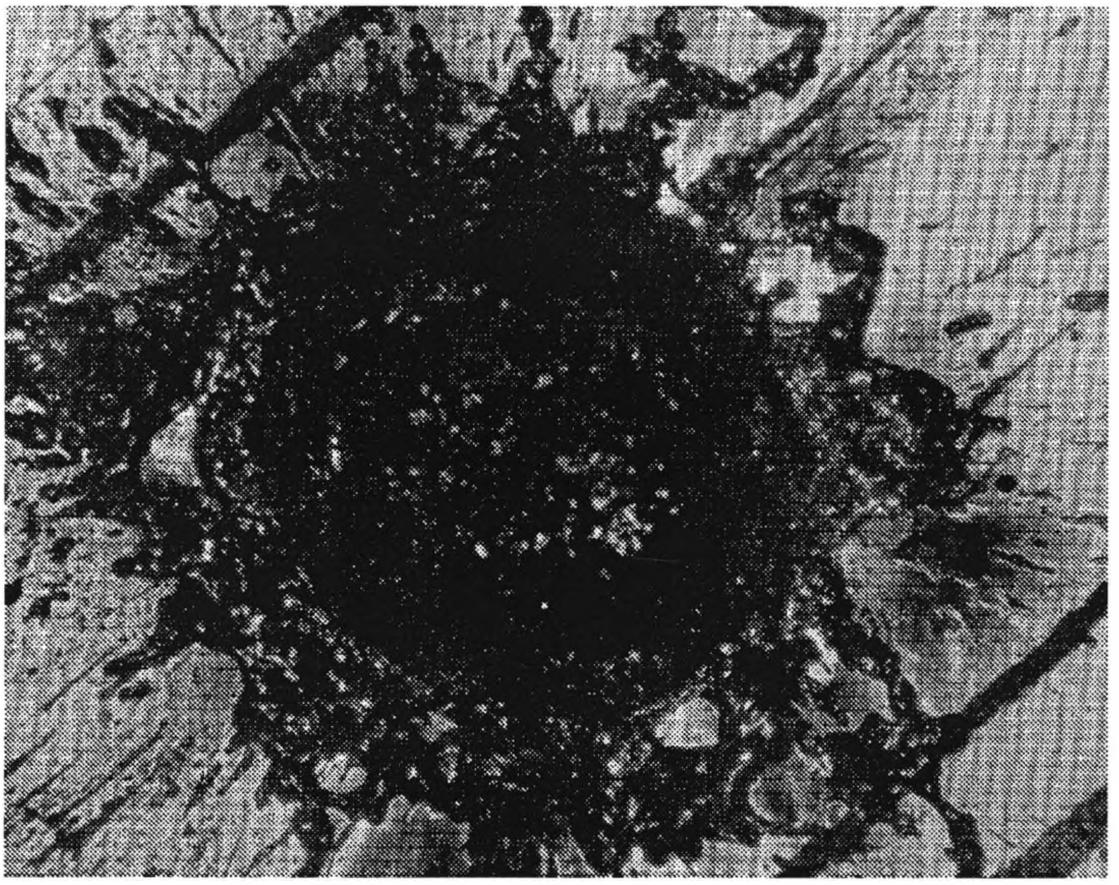

Figure 1.1: Photomicrograph of a gold surface showing the damage caused in region of contact by the passage of a high current. The area of contact is about 10^{-6} cm^2. Magnification $\times 120$ [11].

950°C which is lower than the melting point of gold (1064°C). This temperature can be calculated from the temperature-voltage relation. Further, the metallographic evidence showed clearly that some of the gold had reached the melting point, 1064°C. Later on, the researchers in [13] suggested that at high temperatures the behavior of the contact region can not be precisely described by the accepted theory. They developed a theoretical treatment of the general problem of the electrical contact and heating. In this thesis we developed their theories and clearly explain the phenomena occured in study [11].

Material properties of metals such as thermal conductivity and electrical resistivity are temperature dependent. With increasing temperature, the thermal conductivity of gold decreases [15]. However, there would be a rise in the value of the electrical resistivity of gold when temperature increases [16]. The variations with temperature of the thermal conductivity and electrical resistivity of metals can be expressed by the Wiedemann-Franz Law [10].

1.2 Temperature-dependent properties of gold

Thermal conductivity

The magnitude of thermal conductivity of metals depends on the microscopic structure and tends to vary with temperature. The Thermal conductivity, k, of gold decreases very slowly with increasing temperature (Fig. 1.2) [15].

The thermal conductivity of gold at room temperature (T_0 = 298 K) is 317 W/mK. The following relation shows that how the thermal conductivity varies with temperature,

$$k = k_0(1 - \beta\theta), \tag{1.1}$$

where $\theta = T - T_0$ is the supertemperature, T is absolute temperature and β is the temperature coefficient of the thermal conductivity and $\beta = 2 \times 10^{-4}$ K^{-1} for gold [15].

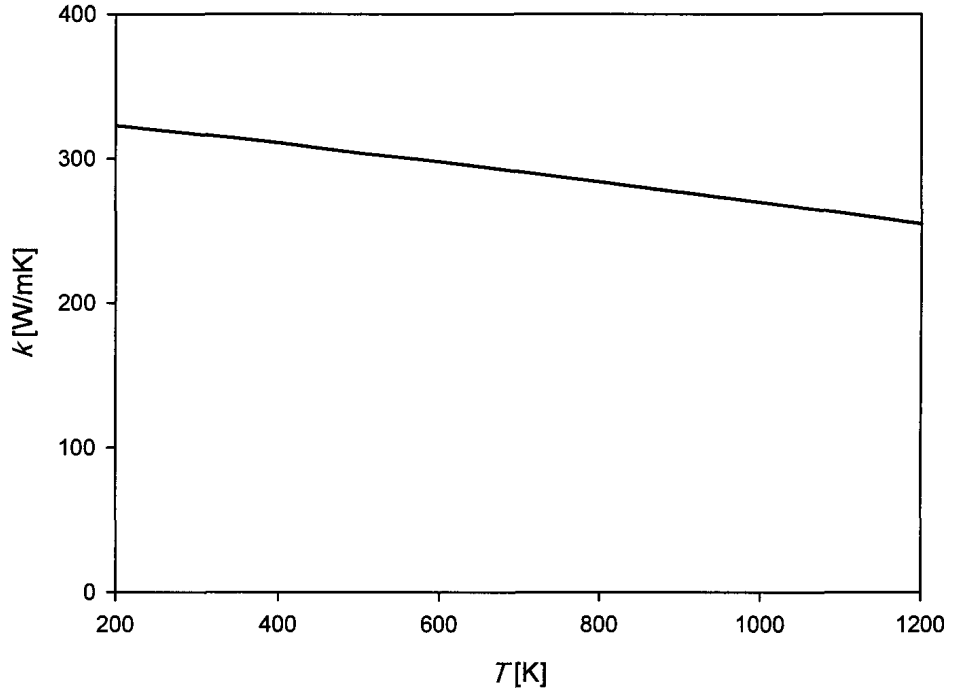

Figure 1.2: Dependance of thermal conductivity of gold on temperature.

Electrical Resistivity

The electrical resistivity of a metal is a function of temperature and increases with increasing temperature. The variation of the electrical resistivity with temperature is linear and can be expressed by [16]

$$\rho = \rho_0(1 + \alpha\theta), \tag{1.2}$$

where ρ_0 is the resistivity at room temperature and α is the temperature coefficient of the electrical resistivity. The magnitude of α for gold is approximately 4×10^{-3} K^{-1}, which is much larger than the temperature coefficient of thermal conductivity, $\beta = 2 \times 10^{-4}$ K^{-1}. Figure 1.3 shows the variaton in electrical resistivity of gold with temperature.

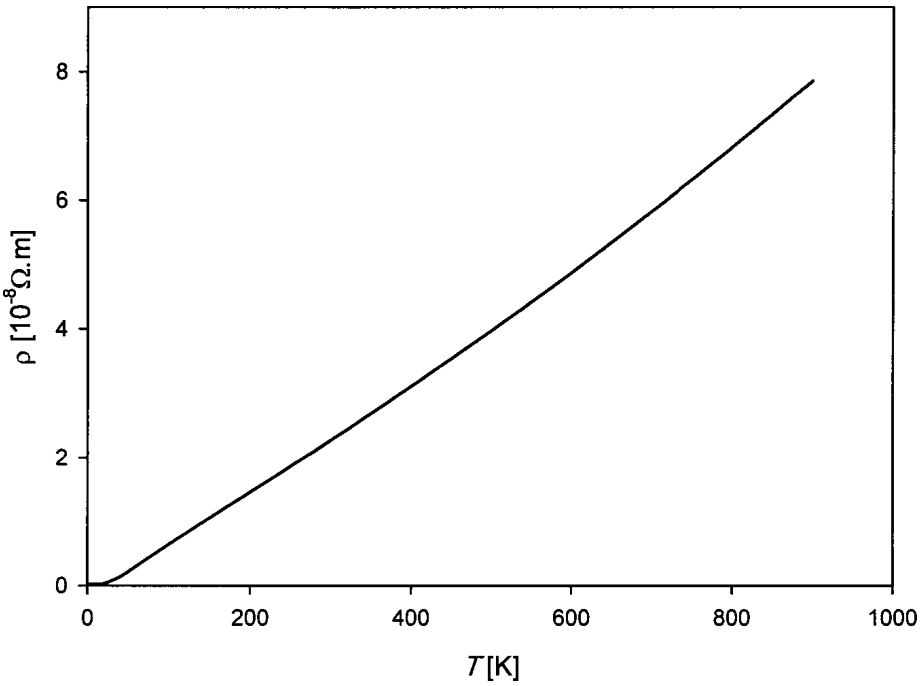

Figure 1.3: Dependance of electrical resistivity of gold on temperature.

The Wiedemann-Franz Law

The Wiedemann-Franz Law [10] states the variations with temperature of the thermal conductivity, k, and the electrical resistivity, ρ, of metals

$$k\rho = L_c T, \tag{1.3}$$

where L_c is the Lorenz constant (2.45×10^{-8} (V/K)^2). This relation holds when thermal conduction and electrical resistivity arise from electronic transport in metals. From this relation we can obtain $k\rho = k_0\rho_0\frac{T}{T_0}$, then using $\theta = T - T_0$, it follows that

$$k\rho = k_0\rho_0\left(1 + \frac{\theta}{T_0}\right). \tag{1.4}$$

The above relation which will be used in the following analysis, states the

relation among the thermal conductivity, the electrical reistivity and the temperature in another form.

1.3 Thesis outline

The approach of this study aims at analysing the interface of a switch or a relay upon passing electrical current through the contact. During pssage of current through the contact, some portions of the interface will melt and weld due to high temperature and a molten metal might be splashed from the surfaces. When the molten metal solidifies, the two surfaces may bond and the device will damage and fail. Even though there is no melting or splashing, high temperature may change mechanical properties of the relay, soften the asperities of the surfaces and make the real contact area larger leading to larger adhesion, which also will cause the failure of the device. The objective of this thesis is to determine the temperature field across contacting surfaces of a MEMS switch contact system which is subject to electric current flow. The objective of this thesis is to determine the maximum possible current and the temperature field across contacting surfaces of a MEMS switch contact system which is subject to electric current flow.

Chapter 2

Current across an a-spot

2.1 Problem configuration

Figure 2.1 shows a model for the problem of electrical flow between two conductors that contact each other over a circular spot, called a-spot [23]. The radius of the spot is a and the thickness of each conductors is L. The potentials at the upper and lower surfaces, which are held at room temperature, are V_0 and $-V_0$, respectively. All electrical currents pass through the a-spot which means the rest of the interface surface is insulated. It is obvious that due to symmetry, the voltage at the a-spot is zero. It is required to determine the values of the potential V, the current I, and the temperature T at all points of the system. The boundary conditions for this problem are

$$\begin{aligned} &V = V_0, && z = L, && \\ &V = -V_0, && z = -L, && \\ &V = 0, && z = 0, && r < a, \\ &\frac{\partial V}{\partial z} = 0, && z = 0, && r > a. \end{aligned} \tag{2.1}$$

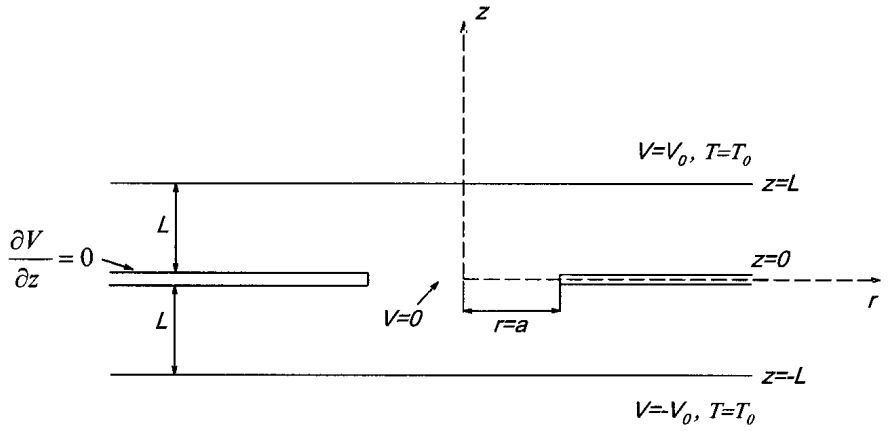

Figure 2.1: Two charged conductors contacting over an a-spot.

2.2 Exact solution

In this section, it is convenient to scale the spatial variables with respect to the contact radius a so that, instead of a, the spot size has unit radius and the thickness is $L^* = L/a$. Proceeding with this in mind, the current density vector is

$$\mathbf{j} = -\sigma \text{ grad } V, \tag{2.2}$$

where σ is the electrical conductivity. From Kirchhoff's law we may write

$$\text{div } \mathbf{j} = -\text{div } (\sigma \text{ grad } V) = 0. \tag{2.3}$$

The above equation indicates that the net electric outflow per unit volume passing through any point within the a-spot system is zero and it holds everywhere inside the system. The equation is nonlinear due to temperature dependence of σ. The temperature rise depends on the voltage and the nonlinearity can be removed if we regard the conductivity as being a function of V instead of T.

Following Carslaw and Jaeger [17], we define a function called ψ as

$$\psi = \int_0^V \sigma d\eta. \tag{2.4}$$

The gradient of the function ψ will be,

$$\text{grad } \psi = \sigma \text{ grad } V = -\mathbf{j},$$

then it is easy to show that ψ satisfies Laplace's equation,

$$\text{div } \mathbf{j} = -\text{div } (\text{grad } \psi) = -\nabla^2\psi = 0, \tag{2.5}$$

so, we have

$$\nabla^2\psi = \frac{\partial^2\psi}{\partial r^2} + \frac{1}{r}\frac{\partial\psi}{\partial r} + \frac{\partial^2\psi}{\partial z^2} = 0. \tag{2.6}$$

The boundary conditions changes to

$$\begin{aligned}
&\psi = \Omega, && z = L^*, && \\
&\psi = -\Omega, && z = -L^*, && \\
&\psi = 0, && z = 0, && r < 1, \\
&\frac{\partial\psi}{\partial z} = 0, && z = 0, && r > 1,
\end{aligned} \tag{2.7}$$

where $\Omega = \int_0^{V_0} \sigma d\eta$. The solution to this problem has the following form

$$\begin{aligned}
\psi &= \Omega\left(1 - \int_0^\infty A(\lambda)\frac{\sinh\lambda(L^* - z)}{\lambda\cosh\lambda L^*}J_0(\lambda r)d\lambda\right) \qquad z > 0, \\
\psi &= -\Omega\left(1 - \int_0^\infty A(\lambda)\frac{\sinh\lambda(L^* + z)}{\lambda\cosh\lambda L^*}J_0(\lambda r)d\lambda\right) \qquad z < 0,
\end{aligned} \tag{2.8}$$

where $A(\lambda)$ is an unknown function and $J_0(\lambda)$ is Bessel's function. Applying the boundary conditions on $z = 0$ leads to the following dual integral equations:

$$\begin{cases} I_1 = \int_0^\infty \lambda^{-1} A(\lambda) \tanh \lambda L^* J_0(\lambda r) d\lambda = 1, & r < 1, \\ \\ I_2 = \int_0^\infty A(\lambda) J_0(\lambda r) d\lambda = 0, & r > 1. \end{cases} \tag{2.9}$$

We represent $A(\lambda)$ in terms of a new function $\phi(t)$ by the equation

$$A(\lambda) = \lambda \int_0^1 \phi(t) \cos \lambda t \; dt. \tag{2.10}$$

Substituting the equation (2.10) into the second of the set (2.9) and using the method of integral by parts, there is

$$I_2 = \phi(1) \int_0^\infty J_0(\lambda r) \sin \lambda d\lambda - \int_{t=0}^1 \phi'(t) dt \int_{\lambda=0}^\infty J_0(\lambda r) \sin \lambda t = 0, \quad r > 1, \tag{2.11}$$

where $'$ indicates the differentiation with respect to t. Using the result of the following relation [18]

$$\int_0^\infty J_0(xr) \sin xt \; dx = \begin{cases} (t^2 - r^2)^{-1/2}, & 0 \le r < t, \\ 0, & r > t, \end{cases} \tag{2.12}$$

it can be shown that $I_2 = 0$ is automatically satisfied.
By defining $f(\lambda) = 1 - \tanh \lambda L^*$, I_1 (Eq. 2.9) converts to

$$\begin{aligned} I_1 &= \int_0^\infty \lambda^{-1} \left[1 - f(\lambda)\right] A(\lambda) J_0(\lambda r) d\lambda \\ &= \int_0^\infty \lambda^{-1} A(\lambda) J_0(\lambda r) d\lambda - \int_0^\infty \lambda^{-1} f(\lambda) A(\lambda) J_0(\lambda r) d\lambda = 1. \end{aligned} \tag{2.13}$$

Calling the first term of I_1 as $\zeta(r)$, and substituting $A(\lambda)$ from the equation (2.10), we have

$$\begin{aligned}
\zeta(r) &= \int_0^\infty \lambda^{-1} A(\lambda) J_0(\lambda r) d\lambda \\
&= \int_{\lambda=0}^\infty \lambda^{-1} \left(\lambda \int_{t=0}^1 \phi(t) \cos \lambda t dt \right) J_0(\lambda r) d\lambda \\
&= \int_{t=0}^1 \phi(t) dt \int_{\lambda=0}^\infty \cos \lambda t J_0(\lambda r) d\lambda \\
&= \int_0^r \frac{\phi(t) dt}{\sqrt{r^2 - t^2)}}, \qquad (2.14)
\end{aligned}$$

in which the following result is used [18]

$$\int_0^\infty J_0(xr) \cos xt \; dx = \begin{cases} 0, & 0 \le r < t, \\ (r^2 - t^2)^{-1/2}, & r > t. \end{cases} \qquad (2.15)$$

Introducing the Erdelyi-Kober operator $I_{\eta,\alpha}$ as following

$$I_{\eta,\alpha} \; g(x) = \frac{2x^{-2\alpha-2\eta}}{\Gamma(\alpha)} \int_0^x (x^2 - u^2)^{\alpha-1} u^{2\eta+1} g(u) du, \qquad (2.16)$$

$\zeta(r)$ can be written as

$$\zeta(r) = \int_0^r \frac{\phi(t) dt}{\sqrt{r^2 - t^2}} = \frac{\sqrt{\pi}}{2} I_{-\frac{1}{2},\frac{1}{2}} \{\phi(t); r\}. \qquad (2.17)$$

From the equation (2.13), we have

$$\frac{\sqrt{\pi}}{2} I_{-\frac{1}{2},\frac{1}{2}} \{\phi(t); r\} = 1 + \int_{\lambda=0}^\infty f(\lambda) J_0(\lambda r) d\lambda \int_{t=0}^1 \phi(t) \cos \lambda t dt. \qquad (2.18)$$

It can be proven that $I_{\eta,\alpha}^{-1} = I_{\eta+\alpha,-\alpha}$ [20]. Multiplying both sides of the above

equation by $\frac{2}{\sqrt{\pi}} I^{-1}_{-\frac{1}{2},\frac{1}{2}}$, yields

$$\phi(t) = \frac{2}{\sqrt{\pi}} I_{0,-\frac{1}{2}} \left\{ 1 + \int_{\lambda=0}^{\infty} f(\lambda) J_0(\lambda r) d\lambda \int_{t=0}^{1} \phi(t) \cos \lambda t dt \right\}. \tag{2.19}$$

Using the definition of $I_{\eta,\alpha}$, we have

$$\begin{aligned} \frac{2}{\sqrt{\pi}} I_{0,-\frac{1}{2}} \{g(t); r\} &= \frac{4t}{\sqrt{\pi}\Gamma(-\frac{1}{2})} \int_0^t (t^2 - r^2)^{-3/2} r g(r) dr \\ &= -\frac{2t}{\pi} \int_0^t \frac{r g(r) dr}{(t^2 - r^2)^{3/2}} \\ &= \frac{2}{\pi} \frac{d}{dt} \int_0^t \frac{r g(r) dr}{(t^2 - r^2)^{1/2}}. \end{aligned} \tag{2.20}$$

Thus, the function $\phi(t)$ in the equation (2.19) becomes

$$\begin{aligned} \phi(t) = \; & \frac{2}{\pi} \frac{d}{dt} \int_0^t \frac{r dr}{(t^2 - r^2)^{1/2}} \\ & + \frac{2}{\sqrt{\pi}} \int_{\lambda=0}^{\infty} f(\lambda) d\lambda \left(\frac{d}{dt} \int_{r=0}^{t} \frac{r J_0(\lambda r) dr}{(t^2 - r^2)^{1/2}} \right) \int_{x=0}^{1} \phi(x) \cos \lambda x dx. \end{aligned} \tag{2.21}$$

Utilizing the well-known relation of [20]

$$\frac{d}{dt} \int_0^t \frac{r J_0(\lambda r) dr}{\sqrt{t^2 - r^2}} = \cos \lambda t, \tag{2.22}$$

the equation (2.21) simplifies to

$$\phi(t) = \frac{2}{\pi} \left(1 + \int_{\lambda=0}^{\infty} f(\lambda) \cos \lambda t d\lambda \int_{x=0}^{1} \phi(t) cos \lambda x dx \right), \tag{2.23}$$

which can be rewritten as

$$\phi(t) = \frac{2}{\pi}\left(1 + \int_0^1 \phi(x)k(t,x)\ dx\right), \tag{2.24}$$

where,

$$k(t,x) = \int_0^\infty f(\lambda)\cos\lambda t\cos\lambda x d\lambda, \tag{2.25}$$

and $f(\lambda) = 1 - \tanh\lambda L^*$.

Equation (2.24) is a Fredholm integral equation of the second kind with the kernel $k(t,x)$. In Appendix B, the kernel is evaluated and is given by the equation (B.9).

Approximation of the Fredholm integral equation

Before examining the Fredholm integral equation, we present some basic ideas connected with numerical integration. Consider a definite integral of the form

$$F = \int_a^b f(x)dx.$$

To find an approximate solution of F we divide the interval $[a,b]$ into $n-1$ equally-spaced subintervals. The points of division are called $x_1, x_2, ..., x_n$, so that the points x_1 and x_n are identified with the end points $x = a$ and $x = b$. The length of each subinterval is $h = x_n - x_{n-1}$.

Rectangle Rule

The simplest method to approximate F is the rectangle rule, which assumes that $f(x)$ is piecewise constant in each subinterval and finds an approximation of F by computing the area of a collection of rectangles whose heights are

determined by the values of $f(x)$. According to this rule, we have

$$\begin{aligned} F_R &= h[f_1 + f_2 + ... + f_{n-2} + f_{n-1}] && \text{Type I} \\ &= h[f_2 + f_3 + ... + f_{n-1} + f_n] && \text{Type II} \end{aligned}$$

where f_i is the value of $f(x)$ at $x = x_i$. The error of the rectangular approximation F_R is in the form [28]

$$E_R = \frac{(b-a)h}{2} f'(p), \qquad a < p < b. \tag{2.26}$$

Depending on using Type I or Type II, two different answers will be obtained, which the error of both is proportional to h.

Trapezoidal Rule

The Trapezoidal rule is another method to approximately evaluate F, in which the integrand $f(x)$ is assumed to be linear in each segment. F_T is sum of the areas of all trapezoids.

$$\begin{aligned} F_T &= h\left[\frac{f_1 + f_2}{2} + \frac{f_2 + f_3}{2} + ... + \frac{f_{n-2} + f_{n-1}}{2} + \frac{f_{n-1} + f_n}{2}\right] \\ &= \frac{h}{2}[f_1 + 2f_2 + ... + 2f_{n-1} + f_n]. \end{aligned} \tag{2.27}$$

It is obvious that this result can be found by averaging Type I and Type II of the rectangle rule. The error of this formula can be expressed as [28]

$$E_T = -\frac{(b-a)h^2}{12} f''(p), \qquad a < p < b. \tag{2.28}$$

The error of the trapezoidal's rule is proportional to h^3, which means that for a given number of subintervals, it is more accurate than the rectangle rule.

Simpson's Rule

The third method that we shall develop is called Simpson's Rule. In this method we approximate $f(x)$ with a collection of arcs from quadratic functions and integrate across each of them. The following quadratic function interpolates the three points of $(x_1, f_1), (x_2, f_2)$, and (x_2, f_2):

$$f = \frac{f_1(x-x_2)(x-x_3)}{(x_1-x_2)(x_1-x_3)} + \frac{f_2(x-x_3)(x-x_1)}{(x_2-x_3)(x_2-x_1)} + \frac{f_3(x-x_1)(x-x_2)}{(x_3-x_1)(x_3-x_2)}$$

If the three interpolating points all lie on the same line, then this function reduces to a linear function. Since $h = x_n - x_{n-1}$, there is

$$\begin{aligned} &\int_{x_1}^{x_3} f(x)dx \\ \approx\ &\frac{1}{2h^2}\int_{x_1}^{x_3} f_1(x-x_2)(x-x_3) + f_3(x-x_1)(x-x_2) - 2f_2(x-x_3)(x-x_1)dx \\ \approx\ &\frac{h}{3}(f_1 + 4f_2 + f_3). \end{aligned}$$

Summing the definite integrals over each interval $[x_{i-2}, x_i]$, for $i = 2, 4, ..., n$, provides the approximation

$$\begin{aligned} &\int_a^b f(x)dx \\ \approx\ &\frac{h}{3}(f_1 + 4f_2 + f_3) + \frac{h}{3}(f_3 + 4f_4 + f_5) + ... + \frac{h}{3}(f_{n-2} + 4f_{n-1} + f_n). \end{aligned} \tag{2.29}$$

By simplifying this sum we obtain the Simpson's approximation scheme as

$$F_S = \frac{h}{3}(f_1 + 4f_2 + 2f_3 + 4f_4 ... + 2f_{n-2} + 4f_{n-1} + f_n). \tag{2.30}$$

In Simpson's rule it is require that the number of subintervals be an even number. The error of Simpson's rule for integration over $[a, b]$ which has been subdivided into $2(n-1)$ subintervals of length h is given by [28]

$$E_S = -\frac{(b-a)h^4}{180} f^{(4)}(p) \qquad a < p < b. \tag{2.31}$$

Although in Simpson's rule the number of subintervals must be even, the error of this method is quite remarkable (in order of $O(h^4)$), which is the reason of the popularity of it for numerical integration.

Fredholm integral equation

A Fredholm integral equation can be approximated by a set of algebraic equations [19]. To solve the integral equation (2.24) numerically, we divide the interval $[0, 1]$ into $n-1$ equally-spaced subintervals with length of $h = \frac{1}{n-1}$. Using rectangle rule, we can write

$$\begin{aligned} \phi(t) &\approx \frac{2}{\pi}\left(1 + h\sum_{j=1}^{n-1} \phi(x_j)k(t, x_j)\right), \qquad \text{Type I,} \\ \phi(t) &\approx \frac{2}{\pi}\left(1 + h\sum_{j=2}^{n} \phi(x_j)k(t, x_j)\right), \qquad \text{Type II.} \end{aligned} \tag{2.32}$$

The equation (2.24) can also be approximated in the form

$$\phi(t) \approx \frac{2}{\pi}\left(1+\sum_{j=1}^{n} D_j \phi(x_j) k(t, x_j)\right) \qquad (i = 1, 2, .., n), \tag{2.33}$$

where the constants D_j are corresponding weighting coefficients with the x_j points. However, approximations are generally obtained by choosing these coefficients in accordance with a formula such as the trapezoidal rule or Simpson's rule. The trapezoidal rule gives

$$\{D_1, D_2, D_3, D_4, ..., D_{n-2}, D_{n-1}, D_n\} = h\left\{\frac{1}{2}, 1, 1, 1, ..., 1, 1, \frac{1}{2}\right\}. \tag{2.34}$$

According to Simpson's rule, which is applicable only if n is odd, the weighting coefficients are

$$\{D_1, D_2, D_3, D_4, ..., D_{n-2}, D_{n-1}, D_n\} = \frac{h}{3}\{1, 4, 2, 4, ..., 2, 4, 1\}. \tag{2.35}$$

If we now require that the two members of (2.33) be equal at each of the n points, we obtain n linear equations

$$\phi(x_i) = \frac{2}{\pi}\left(1+\sum_{j=1}^{n} D_j \phi(x_j) k(x_i, x_j)\right) \qquad (i = 1, 2, .., n), \tag{2.36}$$

in which the n unknowns $\phi(x_1), ..., \phi(x_n)$ specify approximate values of the unknown function $\phi(x)$ at n points.
If we introduce the abbreviations

$$\phi_i = \phi(x_i), \qquad k_{ij} = k(x_i, x_j),$$

where k_{ij} is hence the value of $k(x_i, x_j)$ when $x = x_i$ and $t = x_j$, the required set of equations would be of the form

$$\phi_i = \frac{2}{\pi}\left(1 + \sum_{j=1}^{n} D_j \phi_j k_{ij}\right) \qquad (i = 1, 2, .., n). \tag{2.37}$$

After solving this set of algebraic equations and finding the values of ϕ_i, we proceed to obtain the current passing across the contact spot. Although this set of equations is solved by all the numerical methods mentioned, the results in chapter 5 is given by using Simpson's rule for its small error comparing with the other methods. Tranter has examined the dual integral equation (2.9) by a different method for large values of L^* [21]. The results from this study agree satisfactorily with the Tranter's results when L^* is large.

Current through contact interface

In fact the radius of the spot is a which we took it as unity in the previous calculations. Taking this into account, to find the total current passing through the a-spot, we may write

$$I = 2\pi a \int_0^1 \left.\frac{\partial \psi}{\partial z}\right|_{z=0} r dr. \tag{2.38}$$

According to the set of (2.8), on plane $z = 0$, we have

$$\frac{\partial \psi}{\partial z} = \Omega \int_0^\infty A(\lambda) J_0(\lambda r) d\lambda. \tag{2.39}$$

Substituting the above equation in the equation (2.38) and exchanging the order of integration, we get

$$I = 2\pi a \Omega \int_0^\infty A(\lambda) J_1(\lambda) \frac{d\lambda}{\lambda}. \tag{2.40}$$

Substituting $A(\lambda) = \lambda \int_0^1 \phi(t) \cos \lambda t \, dt$ in the above equation, results

$$I = 2\pi a \Omega \int_0^\infty \cos(\lambda x) J_1(\lambda) d\lambda \int_0^1 \phi(x) dx. \tag{2.41}$$

Using the following result [18]

$$\int_0^\infty \cos(\lambda x) J_1(\lambda) d\lambda = 1, \qquad 0 < x < 1, \tag{2.42}$$

the equation (2.41) simplifies to

$$I = 2\pi a \phi_0 \Omega, \tag{2.43}$$

where $\phi_0 = \int_0^1 \phi(x) dx$ and $\Omega = \int_0^{V_0} \sigma d\eta$, which is evaluated in Appendix A. Utilizing the equation (A.18), we find the current passing across the a-spot as

$$I = 4a\sigma_0 \xi f_a(L^*) V_0, \tag{2.44}$$

where $f_a(L^*)$ is

$$f_a(L^*) = \frac{\pi}{2} \int_0^1 \phi(x) dx, \tag{2.45}$$

and ξ is given in equation (A.19). The a-spot resistance is defined as

$$R_a = \frac{V_0}{I} = \frac{1}{4a\sigma_0 \xi f_a(L^*)} = \frac{R_c}{f_a(L^*)}. \tag{2.46}$$

where $R_c = 1/(4a\sigma_0\xi)$ represents the constriction resistance when L^* becomes infinitely large [13].

Chapter 3

Parallel circuit approximation

Solving the main problem by utilizing the method described in the previous chapter is very complicated and difficult. In this chapter, we present a simple approximate model to obtain the resistance of an a-spot system. To obtain this simple approximation we consider two problems corresponding to the limiting cases when $L \ll a$ and $L \gg a$.

3.1 Current through a metal bar ($L \ll a$)

When $L \ll a$ the heat flow between the upper and lower surfaces will be almost completely one-dimensional. So, in this section we examine the problem of current through a straight metal bar shown in Fig. 3.1. The length of bar is $2L$ with cross-sectional area $A = \pi a^2$; the bar shown in the figure is not drawn to scale. A potential difference of $2V_0$ is applied between the two ends which are held at room temperature ($T_0 = 298$ K), so that $\theta = 0$ at both ends. The material properties of the bar are assumed to be temperature-dependent.

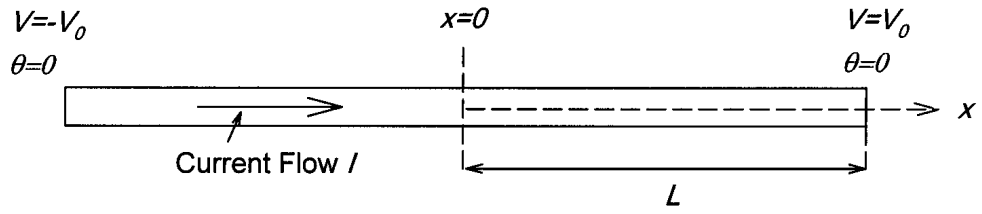

Figure 3.1: Model of an electrified straight metal bar.

The boundary conditions are

$$\begin{aligned} V &= V_0, \quad \theta = 0, \quad x = L, \\ V &= -V_0, \quad \theta = 0, \quad x = -L. \end{aligned} \tag{3.1}$$

It is assumed that the current flows solely in x-direction which means that the bar is thermally insulated along the lateral surface. According Ohm's law, the current density is

$$j_x = -\sigma \frac{dV}{dx}, \tag{3.2}$$

where σ is the electrical conductivity. Applying Kirchhoff's law

$$\frac{dj_x}{dx} = \frac{d}{dx}\left(\sigma \frac{dV}{dx}\right) = 0, \tag{3.3}$$

which states that the net electric outflow per unit volume passing through any point within the bar is zero. Similar to the method mentioned in the previous chapter, we define function ψ as

$$\psi = \int_0^V \sigma d\eta. \tag{3.4}$$

So, we have

$$\frac{d\psi}{dx} = \sigma \frac{dV}{dx} = -j_x = \text{constant}. \tag{3.5}$$

Therefore, ψ satisfies the Laplace's equation, $\nabla^2\psi = 0$, so that $\psi = c_1 x + c_2$, where c_1 and c_2 are constants. Noting that due to symmetry, at $x = 0$ the potential is zero, we have $c_2 = 0$. By applying the boundary conditions at $x = \pm L$ the function ψ is found as

$$\psi = \frac{x}{L}\int_0^{V_0} \sigma d\eta. \tag{3.6}$$

Then, the total current passing through the bar can be obtained by using the following relation

$$I = j_x A = \frac{d\psi}{dx}A = \frac{A}{L}\int_0^{V_0} \sigma d\eta. \tag{3.7}$$

The evaluation of the integral involved in the above equation is presented in Appendix A and the expression for the current I can be written as

$$I = \frac{A}{L}\sigma_0 V_0\ \xi, \tag{3.8}$$

where ξ is given in equation (A.19). The resistance of the bar R_b is then expressed as

$$R_b = \frac{L}{A\sigma_0\xi}. \tag{3.9}$$

When V^* is small, the Joule heating is negligible and $\xi = 1$ so that R_b reduces to the standard form found in elementary textbooks.

3.2 Current across micro-contact spot ($L \gg a$)

A micro-contact system is formed of two large blocks of metal which contact each other over a very small area (Fig. 3.2). The pieces of metal can be modeled as semi-infinite solids ($z > 0, z < 0$). The applied voltage on the far

surfaces $S1$ and $S2$ are V_0 and $-V_0$, respectively, and the current passes only through the spot since the surface $SSSS$ is assumed to be electrically insulated. At the contact spot, due to the configuration symmetry, it is obvious that the voltage is equal to zero ($V = 0$). we take a as the radius of the contact area. The results in this section have previously been deduced by Greenwood and Williams [13] and are reproduced here for the sake of completeness.

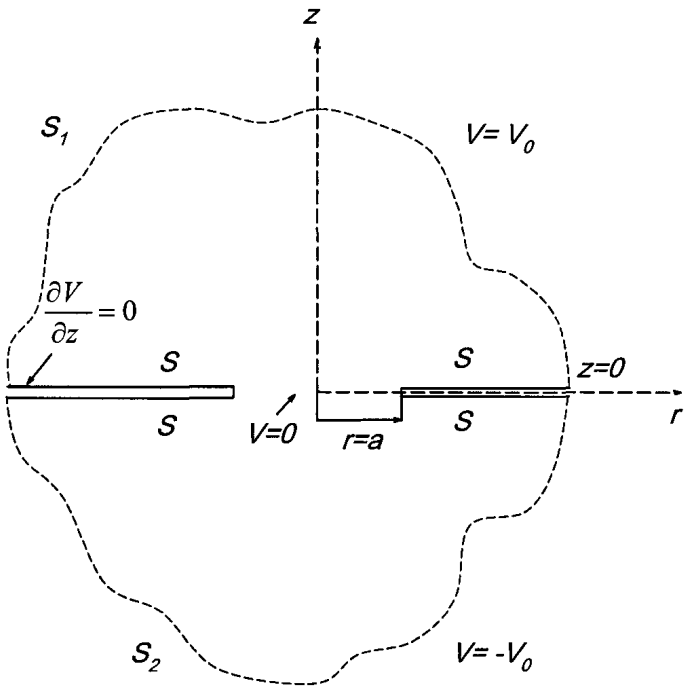

Figure 3.2: Micro-contact system.

The boundary conditions can be summarized as follows

$$\begin{aligned} V &= V_0, & r^2 + z^2 &\to \infty, & z &> 0, \\ V &= -V_0, & r^2 + z^2 &\to \infty, & z &< 0, \\ V &= 0, & r &< a, & z &= 0, \\ \frac{\partial V}{\partial z} &= 0, & r &> a, & z &= 0. \end{aligned} \tag{3.10}$$

It is required to obtain the relation between the current, the potential, and the temperature at the contact region. Applying Ohm's and Kirchhoff's laws and making use of the definition $\psi = \int_0^V \sigma d\eta$, it is easy to show that ψ satisfies the Laplace's equation,

$$\nabla^2 \psi = 0. \tag{3.11}$$

By introducing ψ, the boundary conditions converts to

$$\begin{aligned}
&\psi = \Omega, && r^2 + z^2 \to \infty, && z > 0, \\
&\psi = -\Omega, && r^2 + z^2 \to \infty, && z < 0, \\
&\psi = 0, && r < a, && z = 0, \\
&\frac{\partial \psi}{\partial z} = 0, && r > a, && z = 0.
\end{aligned} \tag{3.12}$$

The solution of the above problem is in the form of [17]

$$\begin{aligned}
\psi &= \Omega \left(1 - \frac{2}{\pi} \int_0^\infty \exp(-\lambda z) J_0(\lambda r) \sin \lambda a \frac{d\lambda}{\lambda} \right) \qquad z > 0, \\
\psi &= -\Omega \left(1 - \frac{2}{\pi} \int_0^\infty \exp(\lambda z) J_0(\lambda r) \sin \lambda a \frac{d\lambda}{\lambda} \right) \qquad z < 0.
\end{aligned} \tag{3.13}$$

So, we have

$$\left. \frac{\partial \psi}{\partial z} \right|_{z=0} = \frac{2\Omega}{\pi} \int_0^\infty J_0(\lambda r) \sin \lambda a d\lambda = \begin{cases} \dfrac{2\Omega}{\pi \sqrt{a^2 - r^2}}, & 0 \le r < a, \\ 0, & r > a. \end{cases} \tag{3.14}$$

The current passing through the micro-contact spot is

$$I = \int_A \mathbf{j} \, dA = \int_A \text{grad } \psi \, dA = 2\pi \int_0^a \left. \frac{\partial \psi}{\partial z} \right|_{z=0} r dr. \tag{3.15}$$

Hence, from equations (3.15) and (3.14), one can obtain the current passing through a micro-contact spot as

$$\begin{aligned} I &= 4\Omega \int_0^a \frac{r dr}{\sqrt{a^2 - r^2}} \\ &= 4a\Omega. \end{aligned} \tag{3.16}$$

Applying the equation (A.18), it is found that

$$I = 4a\sigma_0 V_0 \xi, \tag{3.17}$$

where ξ is given in equation (A.19). The constriction resistance is then

$$R_c = \frac{1}{4a\sigma_0 \xi}. \tag{3.18}$$

For small values of V^*, the expression for R_c reduces to the well-known form for the constriction resistance of a half-space as given, for example, by Carslaw and Jaeger [17].

3.3 Equivalent resistance

Intuitively it is expected that when $L^* \ll 1$ the resistance of an a-spot system will approach R_b while at the other extreme, i.e. when $L^* \gg 1$, the resistance tends to R_c. Here, it is assumed that for intermediate values of L^* the heat flow be some combination of these two modes. So, with this dual-mode heat flow assumption, the approximate resistance is found using a parallel circuit model:

$$\frac{1}{R_d} = \frac{1}{R_b} + \frac{1}{R_c}. \tag{3.19}$$

Substituting the values of R_b and R_c in the above equation, we get

$$R_d = \frac{R_c}{f_d(L^*)}, \tag{3.20}$$

where R_c is given in equation (3.18) and

$$f_d(L^*) = 1 + \frac{\pi}{4L^*}, \tag{3.21}$$

gives the influence of L^* upon the resistance.

Hence, the current can be expressed as

$$\begin{aligned} I &= \frac{V_0}{R_d} \\ &= 4a\sigma_0\xi f_d(L^*)V_0. \end{aligned} \tag{3.22}$$

Chapter 4

Variational calculus

In this chapter we develop a treatment to find a more accurate approximate solution of the main problem (current across an a-spot). For this purpose, we consider the problem as a combination of the cases when the thickness of the contacting conductors, L^*, is very small (a bar) and when L^* is very large (a micro-contact system).

To begin we split flux across the contact into two parts: 1) a fraction f of the total current is due to uniform flow, and 2) the remaining fraction, $(1-f)$, is due to the constriction mode of heat flow. To represent this situation we write

$$\left.\frac{\partial\psi}{\partial z}\right|_{z=0} = \frac{I}{\pi a^2}\begin{cases} f + \dfrac{1-f}{2\sqrt{1-r^2/a^2}}, & 0 \le r < a, \\ 0, & r > a, \end{cases} \tag{4.1}$$

where I and f are found below by minimizing the system energy.

We have shown that the solution ψ which satisfies Laplace's equation and the boundary conditions at $z = \pm L$ has the form given in the equation (2.8),

so that

$$\begin{aligned} \psi &= \Omega\left(1-\int_0^\infty B(\lambda)\left[\frac{\sinh\lambda(L-z)}{\lambda\cosh\lambda L}\right]J_0(\lambda r)d\lambda\right) \qquad z>0, \\ \psi &= -\Omega\left(1-\int_0^\infty B(\lambda)\left[\frac{\sinh\lambda(L+z)}{\lambda\cosh\lambda L}\right]J_0(\lambda r)d\lambda\right) \qquad z<0. \end{aligned} \tag{4.2}$$

These expressions along with (4.1) yields

$$\left.\frac{\partial\psi}{\partial z}\right|_{z=0} = \Omega\int_0^\infty B(\lambda)J_0(\lambda r)d\lambda = \frac{I}{\pi a^2}\left\{f+\frac{1-f}{2\sqrt{1-r^2/a^2}}\right\}, \qquad r<a. \tag{4.3}$$

Using the results of the relation (2.12) and the following well-known integral [17]

$$\int_0^\infty J_0(\lambda r)J_1(\lambda a)d\lambda = \begin{cases} 0, & r>a, \\ 1/(2a), & r=a, \\ 1/a, & r<a, \end{cases} \tag{4.4}$$

we find an expression for $B(\lambda)$ as

$$B(\lambda) = \frac{I}{\pi a\Omega}\left[fJ_1(\lambda a)+\frac{(1-f)}{2}\sin\lambda a\right]. \tag{4.5}$$

Then, we set up an integral J that represents the power dissipation of the system

$$J = \pi\int_{r=0}^\infty\int_{z=0}^L\left(\psi_r^2+\psi_z^2\right)\,rdrdz + 2\pi\int_0^a \psi\psi_z\Big|_0 rdr, \tag{4.6}$$

where ψ_r and ψ_z indicate derivative of ψ with respect to r and z, respectively. It is not difficult to show that the conditions under which J attains its absolute minimum represents the exact solution to the problem. Here, the flux across the contact plane is prescribed and a local minimum for J is to be found.

Integrating by parts, it is easy to prove the followings:

$$\begin{cases} \int \psi_z^2 dz = \psi\psi_z - \int \psi\psi_{zz} dz, \\ \\ \int \psi_r^2 r dr = \psi\psi_r r - \int \psi(\psi r)' dr, \end{cases} \tag{4.7}$$

where $'$ denotes derivative with respect to r. Making use of the above relations and noting that $\nabla^2\psi = 0$, the equation (4.6) reduces to

$$J = \pi \int_0^\infty \psi\psi_z\Big|_L r dr + \pi \int_0^a \psi\psi_z\Big|_0 r dr. \tag{4.8}$$

The first term on the right hand side of the above equation can be found on the plane $z = L$ as follows

$$\pi \int_0^\infty \psi\psi_z\Big|_L r dr = \frac{I\Omega}{a^2} \int_0^a \left[f + \frac{1-f}{2\sqrt{1 - r^2/a^2}} \right] r dr = \frac{I\Omega}{2}, \tag{4.9}$$

and also the second term in the equation (4.8) on plane $z = 0$ simplifies to

$$\pi \int_0^\infty \psi\psi_z\Big|_0 r dr = \frac{I\Omega}{2} + \frac{I\Omega}{a} \int_0^\infty B(\lambda) \tanh \lambda L \left(f J_1(\lambda a) + \frac{(1-f)}{2} \sin \lambda a \right) \frac{d\lambda}{\lambda^2}, \tag{4.10}$$

where $B(\lambda)$ is given in the equation (4.5). So, the equation (4.8) converts to

$$\begin{aligned} J \;=\; & I\Omega - \frac{I^2}{\pi a^2} \left[f^2 \int_0^\infty J_1^2(\lambda a) \tanh \lambda L \frac{d\lambda}{\lambda^2} + \int_0^\infty J_1(\lambda a) \sin \lambda a \tanh \lambda L \frac{d\lambda}{\lambda^2} \right. \\ & \left. + \frac{(1-f)^2}{4} \int_0^\infty \sin^2 \lambda a \tanh \lambda L \frac{d\lambda}{\lambda^2} \right]. \end{aligned} \tag{4.11}$$

Defining Y, U and W as

$$\begin{aligned} Y &= \int_0^\infty J_1^2(\xi)\tanh\xi L^* \frac{d\xi}{\xi^2}, \\ U &= \int_0^\infty J_1(\xi)\sin\xi\tanh\xi L^* \frac{d\xi}{\xi^2}, \\ W &= \int_0^\infty \sin^2\xi\tanh\xi L^* \frac{d\xi}{\xi^2}, \end{aligned} \tag{4.12}$$

the J-integral simplifies to

$$J = I\Omega - \frac{I^2}{\pi a}\left[f^2 Y + (f - f^2)U + \frac{(1-f)^2}{4}W\right]. \tag{4.13}$$

Then we minimize the energy of the a-spot system. So, the derivative of J must be zero with respect to both f and I.

$$\frac{\partial J}{\partial f} = 0 \quad \Rightarrow \quad -\frac{I^2}{\pi a}\left[2fY + (1-2f)U - \frac{1-f}{2}W\right] = 0, \tag{4.14}$$

thus, the current flow fraction, f, can be found as following

$$f = \frac{W - 2U}{4Y - 4U + W}. \tag{4.15}$$

Making use of $\dfrac{\partial J}{\partial I} = 0$, we can obtain the current passing through the spot

$$I = \frac{2\pi a\Omega}{4f^2Y + 4(f - f^2)U + (1-f)^2W}. \tag{4.16}$$

Utilizing equations (A.18) and (A.19), the above relation converts to

$$I = 4a\sigma_0\xi f_e(L^*)V_0, \tag{4.17}$$

where $f_e(L^*)$ is defined as

$$f_e(L^*) = \frac{\pi/2}{4f^2Y + 4(f - f^2)U + (1 - f)^2W}. \tag{4.18}$$

Now we introduce an approximate resistance R_e as following

$$R_e = \frac{V_0}{I} = \frac{1}{4a\sigma_0\xi f_e(L^*)} = \frac{R_c}{f_e(L^*)}. \tag{4.19}$$

As L^* becomes large $f_e(L^*) \approx 1$ and the resistance tends to R_c.

Figure 4.1 shows the variation of the current flow fraction f with the dimensionless thickness. When L^* is very small, a significant value of current which is dominantly uniform passes through the spot. In this case, from the equation (4.15), it can be found that $f \sim 1$ and also equation (4.16) gives $I \sim \pi a\Omega/L^*$, which is the same as the result of the analysis of a metal bar. As L^* gets larger, the constriction mode of current flow increases, so the values of f decreases. When $(L^* \to \infty)$, the current flow fraction approaches zero and $I \sim 4a\Omega$ which matches with the analysis of micro-contact system. This figure gives a useful scheme to approximate an a-spot system with either a bar or a micro-contact system, depending on the required accuracy, to avoid the complicated computations described in chapter 2.

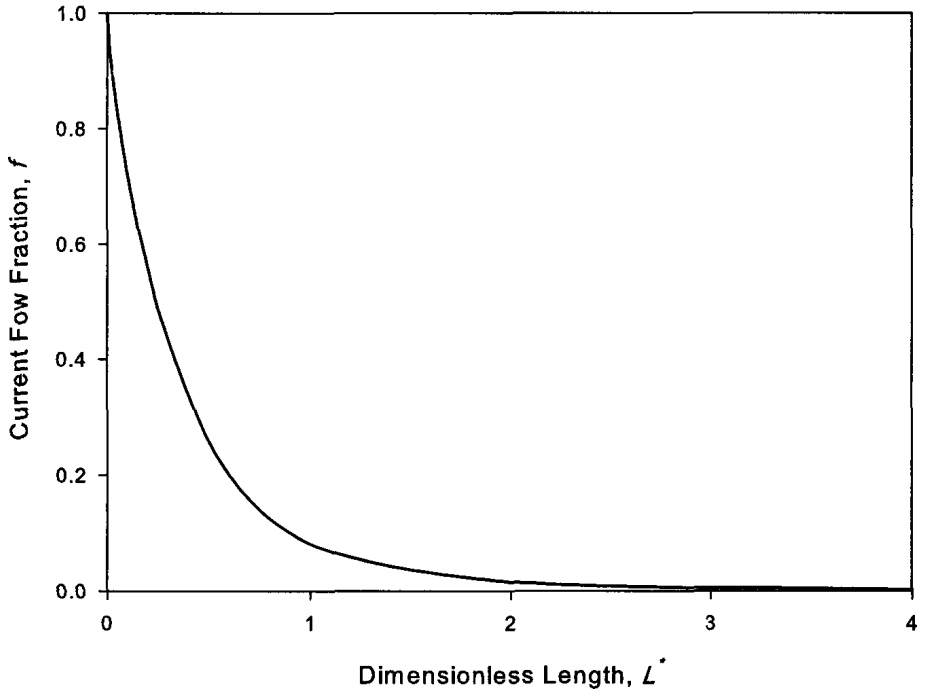

Figure 4.1: Effect of dimensionless thickness on current flow fraction.

Chapter 5

Results and discussion

In this chapter the following features of the analysis are discussed:

1. The approximate models for the resistance are compared with the exact results;
2. Results showing the current-voltage relationship are presented;
3. An expression for the maximum possible current is given;
4. Relationship between voltage and super-temperature is derived;
5. The variation of super-temperature with current is illustrated;
6. The spatial distribution of the voltage and the temperature is depicted.

Validity of the approximations

It has been previously shown in equations (2.46), (3.20), and (4.19), that the form of the resistance is

$$R = \frac{R_c}{f(L^*)}, \tag{5.1}$$

where $f(L^*)$ depends on the method of calculation. It is of interest to compare the two approximations, R_d and R_e, with the exact result R_a. Figure 5.1 shows a graph of R/R_c $(= 1/f(L^*))$ versus L^*. For very small values of L^* the resistance $R/R_c \sim 4L^*/\pi$ corresponding to current flow in a bar. In contrast, as L^* becomes very large, $R/R_c \sim 1$. Away from these two extreme cases, the resistance $R_d < R_a$. However, it does give a reasonable approximation (within about a 10% error) and is a useful result because of its simplicity. The second approximation, R_e, which is found by utilizing the variational method, is virtually indistinguishable from the exact solution. It is notable that this figure is also valid when the electrical conductivity of the medium is a constant.

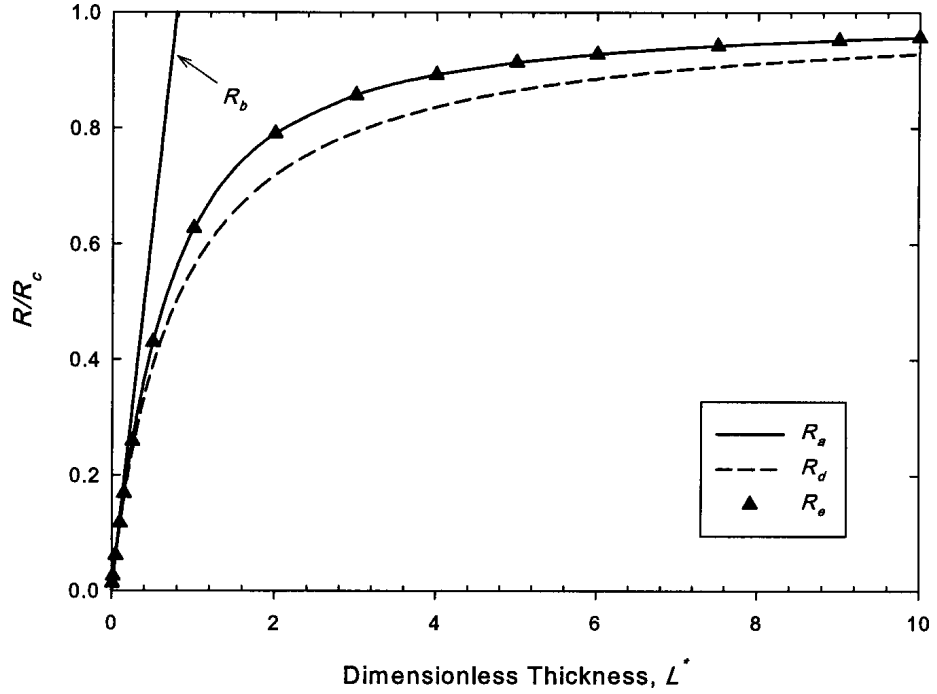

Figure 5.1: Influence of L^* on R/R_c.

Current-voltage relationship

The theoretical relationship between the current passing across a contacting spot with the applied voltage is given in the equations (2.44, 3.22 and 4.17). Introducing dimensionless voltage $V_0^* = V_0/U_0$, this relation can be expressed as

$$I = 4a\sigma_0 U_0 f(L^*)\chi = I_0 f(L^*)\chi, \tag{5.2}$$

where $\chi = \xi V_0^*$ and $I_0 = 4a\sigma_0 U_0$. Now we define a dimensionless current I^* as

$$I^* = \frac{I}{I_0 f(L^*)} = (1+\tau)\arctan V_0^* - \tau V_0^*. \tag{5.3}$$

For small values of V_0^* the Joule heating is negligible and $I_0 \approx V_0^*$. At higher values of V_0^* the behaviour becomes non-linear. Figure 5.2 demonstrates the $I^* - V_0^*$ curve for an a-spot system of gold. Increasing the applied voltage leads to an increase in the current value (Ohm's law) and the medium's temperature increases due to Joule heating. The reason of rise in temperature is the interactions between the moving particles that form the current (electrons) and the atomic ions that make up the body. At the beginning of the curve where the temperature is low, the current varies with the applied voltage almost linearly, which is because in that region, the changes in the value of electrical resistivity, ρ, is small, so that the case can be considered as a problem with the constant electrical resistivity. Since the electrical conductivity varies significantly in higher temperatures, the slope of the curve decreases when approaching to the peak (instability point). At the instability point, the maximum value of current passes through the spot. If the applied voltage is kept further increasing, the current reduces until reaching to the melting point

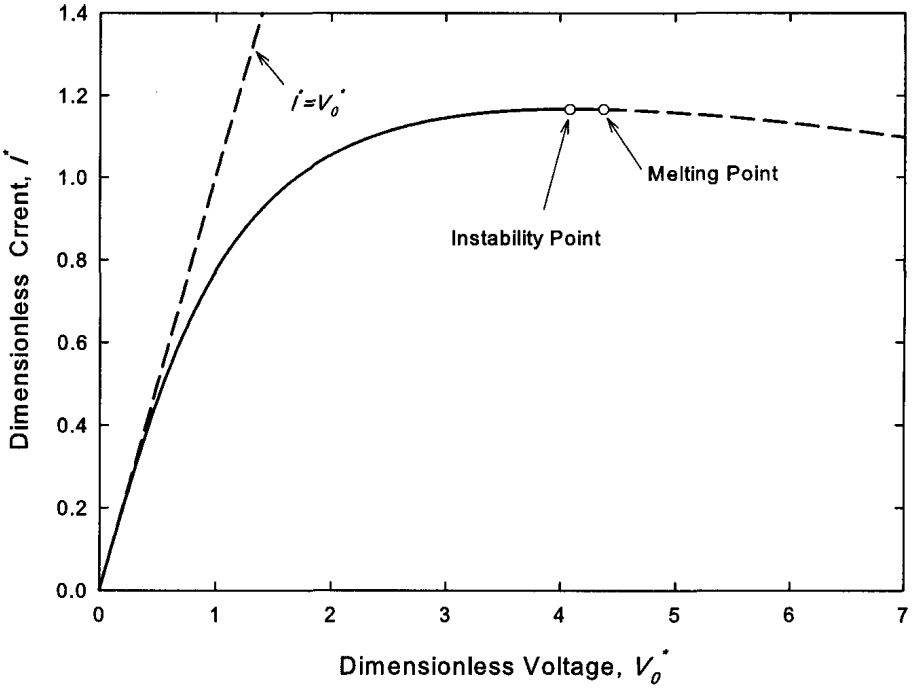

Figure 5.2: Theoretical relation between dimensionless current and voltage for an a-spot system of gold.

where the maximum temperature occurs (1064°C for gold).

Maximum possible current for a given value of L^*

The steady conditions are possible only when the current is below an critical value. If a current greater than this value is maintained the temperature will rise continously and the medium melts. Figure 1.1 shows a molten gold which has splashed from micro-contact interfaces onto the surrounding metal, due to passage of high current. So, it is important to know the maximum possible current passing through the contact spot.

From the equation (5.3), we may write

$$\frac{dI^*}{dV_0^*} = \frac{1 - \tau V_0^{*2}}{1 + V_0^{*2}}, \tag{5.4}$$

Therefore, the maximum dimensionless current is found as

$$I^*_{max} = (1 + \tau) \arctan \frac{1}{\sqrt{\tau}} - \sqrt{\tau}, \tag{5.5}$$

It is obvious that I^*_{max}, which is the dimensionless current corresponding to the instability point, is independent of the geometry of the contacting system and only depends on the properties of the medium. The value of I^*_{max} for a contacting system of gold is $I^*_{max} = 1.17$. Using the definition of I^*, we may write

$$I_{max} = I_0 \left[(1 + \tau) \arctan \frac{1}{\sqrt{\tau}} - \sqrt{\tau} \right] f(L^*), \tag{5.6}$$

which shows the dependence of the maximum current on the properties of the medium and the geometry of the system.

The curve shown in figure 5.2 can be implemented by applying a voltage across an micro-contact system from a low impedance source and keeping increasing the voltage [13]. A low impedance source, also called a voltage source, is a circuit component that supplies a fixed potential difference across its terminals that is almost completely independent of the current it supplies. The internal impedance of such a device is very low. Conversely, a high impedance source, also called a current source, supplies constant current irrespective of the voltage needed by the load across its terminal. The voltage across an ideal current source is completely determined by the circuit connected to the source [14]. If a micro-contact system is connected to a high impedance circuit where the current is slowly increased and potential difference is observed, the curve

would interrupt at instability point [13], i.e. the contact system collapses when the current keeps increasing after instability point even though the maximum temperature at the contact spot does not reach the melting point of gold. This can be used to explain the reason that, in study [11], the contact region collapsed when the temperature was still below the melting point of gold.

The instability point in figure 5.2 is similar to the necking point in a uniaxial tensile test. In a tensile test, the onset of non-uniform plastic deformation (necking) occurs at the necking point where the maximum or ultimate load is carried by the specimen. The relationship between the applied voltage and the current passing through an a-spot is analogous with stress-strain relation in a tensile test. Therefore, we call this point "Instability point" where the current reaches its maximum value and instability occurs.

Figure 5.3 depicts the variation of current and voltage at different room temperatures. At the lower room temperatures, the greater values of applied voltage is required to reach the instability and melting points, and the values of maximum current passing through contact spot is greater than that in higher room temperatures.

Relationship between voltage and super-temperature

Using the Kohlrausch relation (Eq. A.5) and noting that due to the configuration symmetry, the voltage at the contact spot is zero ($V = 0$), it is deduced that the maximum super-temperature occurs exactly at the contact spot. The maximum super-temperature, θ_m, depends on the applied voltage V_0 and also electrical resistivity and thermal conductivity of the medium at room temperature and it is independent of the size of spot. Defining dimensionless super-temperature, θ_m^*, as $\theta_m^* = \theta_m/T_0$, the equation (A.11) becomes

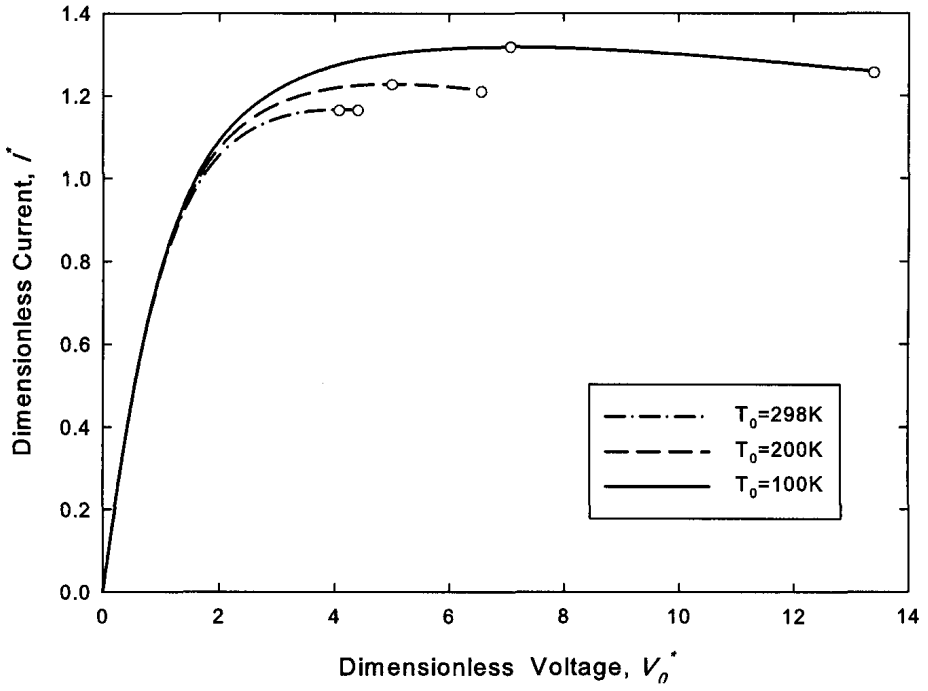

Figure 5.3: Theoretical relation between current and voltage at different room temperature.

$$V_0^{*2} = \theta_m^{*\,2} + 2\theta_m^*. \tag{5.7}$$

The variation of dimensionless super-temperature with dimensionless voltage for an a-spot system of gold is shown in Figure 5.4. Since the maximum super-temperature is independent of the size of the medium, this figure is also valid for the cases of gold bar and micro-contact system of gold. In real conditions, the process stops at the temperature corresponding to the melting point of gold (1064°C), since there is no steady value possible above this temperature.

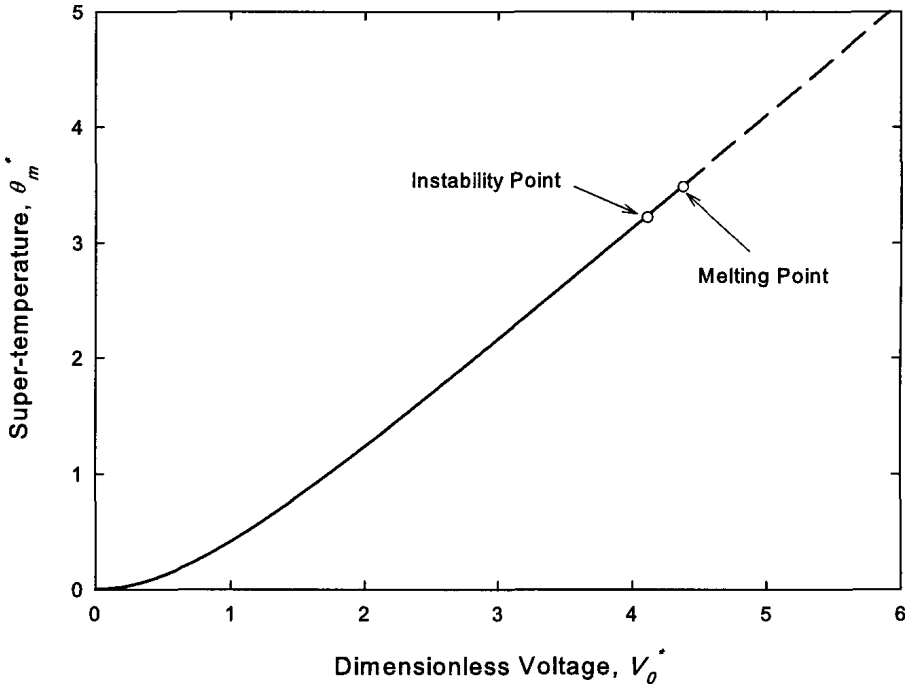

Figure 5.4: Theoretical relation between dimensionless super-temperature and dimensionless voltage in an a-spot system.

Relationship between current and super-temperature

As mentioned before, an increase in the value of the current gives a rise to the kinetic or vibrational energy of the medium's ions, leading to increase in the temperature (Joule heating). Figure 5.5 demonstrates the variation of the temperature at the contact spot with the current passing through it. If the current is kept continuously increasing, the maximum super-temperature increases until reaching the melting point. However, if the current is increased by a high impedance circuit, the instability point would be the last point of the process and any increase in the value of current beyond this point leads to failure of the system.

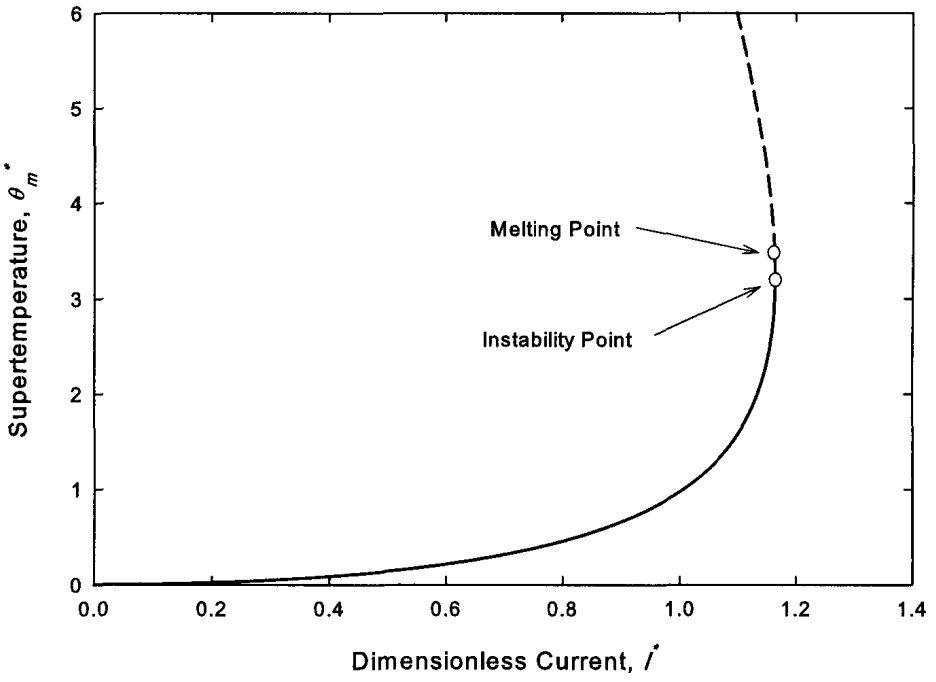

Figure 5.5: Theoretical relation between dimentionless super-temperature and current for an a-spot system of gold.

Distribution of voltage and temperature

Figures 5.6 illustrates the distribution of the temperature along z-axis in a contacting system of gold, when $\theta_m = 1000°C$. It is obvious from the figure that with increasing L^*, the values of the temperature along z-axis decreases.

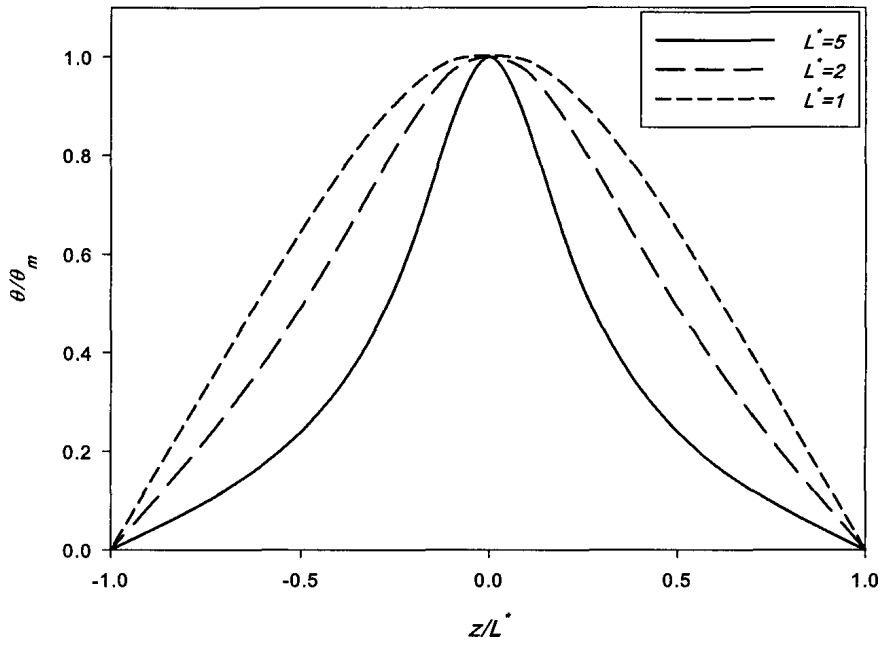

Figure 5.6: Distribution of temperature along z-axis within an a-spot system, for $\theta_m = 1000°\mathrm{C}$.

Chapter 6

Conclusion and contribution

MEMS switch contacts are examined in this study by using the theory of electrically heated bodies. The followings are concluded from this study

1. Stable conditions are possible only when the current is below I_{max}, which is the current corresponding to the instability point. If a current greater than this critical value is maintained the temperature will rise continuously and the medium explodes. An expression for the maximum possible current is been found, equation (5.6), which shows the influence of plate thickness L upon the maximum current.

2. The relation between maximum temperature, θ_m, and applied voltage, V_0, is given by equation (A.11); there is no geometric dependence.

3. It is demonstrated that the a-spot resistance R_a approaches R_b for small values of L^* and tends to R_c when L^* is large. R_d, which is obtained by using a parallel resistance circuit model, underestimates the resistance of the system, leading to obtain a current greater than the actual one. R_d gives an error within almost 10% but it is useful for its simplicity.

4. The use of variational calculus provides an accurate approximate solution and when $L^* > 2$ the electric flow pattern is almost in the pure constriction mode.

Appendix A

Temperature-dependent conductivities

When an electrical current passes through a resistor, the Joule heating leads to the temperature change. In three-dimentional condition, heat flux vector is

$$\mathbf{q} = -k \text{ grad } \theta, \tag{A.1}$$

where k is the thermal conductivity, grad indicates the gradient, and θ is the super-temperature. The heat outflow from volume dv is

$$\text{div}\mathbf{q} \; . \; dv = dP, \tag{A.2}$$

where P is electrical power and div represents the divergence. The electrial power generated in volume $dxdydz$ is

$$\begin{aligned} dP &= I_x^2 R_x + I_y^2 R_y + I_z^2 R_z \\ &= (j_x A_x)^2 \frac{dx}{A_x \sigma} + (j_y A_y)^2 \frac{dy}{A_y \sigma} + (j_z A_z)^2 \frac{dz}{A_z \sigma}. \end{aligned} \tag{A.3}$$

where $A_x = dydz$, $A_y = dzdx$ and $A_z = dxdy$. Making use of the Ohm's law $\mathbf{j} = -\sigma$ grad V, the equation (A.2) becomes

$$\text{div}\,(k \text{ grad } \theta) = -\sigma\ (\text{grad } V)^2, \tag{A.4}$$

which states that in steady conditions, heat generation rate inside any volume is equal to heat rate passing through the surface.

Kohlrausch's relation

The relation between the temperature and the potential at any point of a conductor can be provided by Kohlrausch's relation [13]:

$$V^2 = 2\int_{\theta}^{\theta_m} \rho k d\eta, \tag{A.5}$$

where θ_m is maximum super-temperature and ρ is electrical resistivity. To verify the Kohlrausch's relation, we take gradient of it

$$2V\text{grad } V = -2\rho k \text{ grad } \theta. \tag{A.6}$$

Multiply both side by $\sigma = 1/\rho$, gives

$$\sigma V\text{grad } V = -k \text{ grad } \theta. \tag{A.7}$$

If we take divergence of both side of the above equation, we obtain

$$V\text{div}(\sigma\text{grad } V) + \sigma(\text{grad } V)^2 = -\text{div}\,(k \text{ grad } \theta)\,, \tag{A.8}$$

Using the Ohm's law ($\mathbf{j} = -\sigma \text{ grad } V$) and then the Kirchhoff's law ($\text{div } \mathbf{j} = 0$), the above equation simplifies to

$$\text{div } (k \text{ grad } \theta) = -\sigma \text{ (grad } V)^2. \tag{A.9}$$

Therefore, the governing differential equation (A.4) is satisfied.

σ as a function of V

To solve a general problem of finding the values of current and the potential in a medium with temperature-dependent conductivities we need to find the electrical conductivity as a function of potential. For this purpose, first we substitute $k\rho = k_0\rho_0(1 + \theta/T_0)$ in the equation (A.5),

$$\begin{aligned} V^2 &= 2k_0\rho_0 \int_\theta^{\theta_m} \left(1 + \frac{\eta}{T_0}\right) d\eta \\ &= 2k_0\rho_0 \left[\eta + \frac{\eta^2}{2T_0}\right]_\theta^{\theta_m} \end{aligned} \tag{A.10}$$

Applying boundary condition from equation (3.1) leads to get the relation between applied voltage and maximum super-temperature,

$$V_0^2 = 2k_0\rho_0 \left[\theta_m + \frac{\theta_m^2}{2T_0}\right], \tag{A.11}$$

and the equation (A.10) can be written as

$$V^2 = V_0^2 - 2k_0\rho_0 \left[\theta + \frac{\theta^2}{2T_0}\right], \tag{A.12}$$

which by using $\theta = -T_0\left(1 - \frac{k\rho}{k_0\rho_0}\right)$, converts to

$$V^2 = V_0^2 + 2T_0k_0\rho_0\left[1 - \left(\frac{k\rho}{k_0\rho_0}\right)^2\right]. \tag{A.13}$$

Let $U_0^2 = T_0k_0\rho_0$, this gives the result

$$\frac{k\rho}{k_0\rho_0} = \frac{\sqrt{U_0^2 + V_0^2 - V^2}}{U_0}. \tag{A.14}$$

Applying the relations of $k = k_0(1 - \beta\theta)$ and $\rho = 1/\sigma$, we find an expression for σ as following

$$\sigma = \frac{U_0\sigma_0(1 - \beta\theta)}{\sqrt{U_0^2 + V_0^2 - V^2}}. \tag{A.15}$$

Substituting θ from the following relation

$$\theta = \frac{T_0\sqrt{U_0^2 + V_0^2 - V^2}}{U_0} - T_0, \tag{A.16}$$

into the equation (A.15) and defining $\tau = \beta T_0$, we obtain the relationship between electrical conductivity and potential

$$\sigma = \frac{U_0\sigma_0(1 + \tau)}{\sqrt{U_0^2 + V_0^2 - V^2}} - \sigma_0\tau. \tag{A.17}$$

Ω-Integral

Integral $\Omega = \int_0^{V_0} \sigma d\eta$ is used several times in this study and it is given by

$$\begin{aligned} \Omega &= \sigma_0U_0(1 + \tau)\int_0^{V_0} \frac{d\eta}{\sqrt{U_0^2 + V_0^2 - V^2}} - \sigma_0\tau V_0 \\ &= \sigma_0V_0\,\xi, \end{aligned} \tag{A.18}$$

where ξ is defined as

$$\xi = \frac{(1+\tau)\arctan V_0^*}{V_0^*} - \tau \tag{A.19}$$

and $V_0^* = V_0/U_0$ is the dimensionless voltage. It is clear that when $V_0^* \ll 1$ the function ξ tends to unity.

Appendix B

The kernel of the Fredholm integral equation

To solve the Fredholm integral equation (2.24) we first need to evaluate the kernel integral $k(t,x)$, which is given by

$$k(t,x) = \int_0^\infty (1 - \tanh \lambda L^*) \cos \lambda t \cos \lambda x d\lambda. \tag{B.1}$$

By changing variable as $u = \lambda L^*$ and making use of the following relation

$$\cos \lambda t \cos \lambda x = \frac{1}{2} \left[\cos \lambda (t+x) + \cos \lambda (t-x)\right], \tag{B.2}$$

$k(t,x)$ converts to

$$\begin{aligned} k(t,x) &= \frac{1}{2L} \int_0^\infty (1 - \tanh u) \left\{ \cos u \left(\frac{t+x}{L^*} \right) + \cos u \left(\frac{t-x}{L^*} \right) \right\} du \\ &= \frac{1}{2L} \left\{ \int_0^\infty (1 - \tanh u) \cos u \left(\frac{t+x}{L^*} \right) du + \int_0^\infty (1 - \tanh u) \cos u \left(\frac{t-x}{L^*} \right) du \right\} \\ &= \frac{1}{2L} \left\{ H\left(\frac{t+x}{L^*} \right) + H\left(\frac{t-x}{L^*} \right) \right\}, \end{aligned} \tag{B.3}$$

where function H is of the type

$$H(c) = \int_0^\infty (1 - \tanh x) \cos cx \; dx, \tag{B.4}$$

and $c = (t \pm x)/L^*$. It is clear that $H(c) = H(-c)$ so that the kernel is symmetric. Using the method of integration by parts, yields

$$H(c) = \ln 2 - c \int_0^\infty \sin cx \ln(1 + e^{-2x}) dx. \tag{B.5}$$

The second term on the right is evaluated as [18]

$$\int_0^\infty \sin cx \ln(1 + e^{-2x}) dx = \frac{1}{4c} \left[4 \ln 2 - \psi\left(1 + i\frac{c}{4}\right) - \psi\left(1 - i\frac{c}{4}\right) + \psi\left(\frac{1}{2} + i\frac{c}{4}\right) + \psi\left(\frac{1}{2} - i\frac{c}{4}\right) \right],$$

where the function $\psi(z)$ is defined as

$$\psi(z) = \frac{\Gamma'(z)}{\Gamma(z)},$$

and $\Gamma(z)$ is Gamma function. Therefore, $H(c)$ simplifies to

$$H(c) = \frac{1}{4} \left[\psi\left(1 + i\frac{c}{4}\right) + \psi\left(1 - i\frac{c}{4}\right) - \psi\left(\frac{1}{2} + i\frac{c}{4}\right) - \psi\left(\frac{1}{2} - i\frac{c}{4}\right) \right]. \tag{B.6}$$

By defining a function $\beta(z)$ as

$$\beta(z) = \frac{1}{2} \left[\psi\left(\frac{z+1}{2}\right) - \psi\left(\frac{z}{2}\right) \right], \tag{B.7}$$

the equation (B.6) reduces to

$$H(c) = \frac{1}{2}\left[\beta\left(1 + i\frac{c}{4}\right) + \beta\left(1 - i\frac{c}{4}\right)\right]. \tag{B.8}$$

Using the above expression along with the equation (B.3), we find $k(t, x)$ as

$$\begin{aligned} k(t,x) = \frac{1}{4L^*}\Big[&\beta\left(1 + i\frac{t+x}{4L^*}\right) + \beta\left(1 - i\frac{t+x}{4L^*}\right) \\ &+ \beta\left(1 + i\frac{t-x}{4L^*}\right) + \beta\left(1 - i\frac{t-x}{4L^*}\right)\Big]. \end{aligned} \tag{B.9}$$

Considering the following relations [18]

$$\begin{aligned} \Im\ \psi(1 + ix) &= -\frac{1}{2x} + \frac{\pi}{2}\coth \pi x, \\ \Im\ \psi(\frac{1}{2} + ix) &= \frac{\pi}{2}\tanh \pi x, \end{aligned} \tag{B.10}$$

it is easy to prove that the imaginary part of $k(t, x)$ is zero.

Appendix C

Numerical analysis (Maple)

```
# Solving the Fredholm integral equation by the rectangular rule
  (Type I)

with(LinearAlgebra):

L:=2:   # L is the dimensionless thickness
n:=20:  # n is the number of points. The fist point is x(1).
N:=n-1: # N is the number of intervals
h:=1/N: # h is the length of each interval

# x is the vector of the points between 0 and 1

for i from 1 to N do  # x(i) starts from x(1)=0 to x(N)=1-h
  x(i):=h*(i-1):
end do:
```

```
K:=Matrix(n-1):  # K matrix is the matrix of kernel integral

for i from 1 to N do
 for j from 1 to N do

c1:=(x(i)+x(j))/L:
c2:=(x(i)-x(j))/L:

J1:=-1/4*(Psi(1/2+c1*I/4)+Psi(1/2-c1*I/4)-Psi(1+c1*I/4)
          -Psi(1-c1*I/4)):
J2:=-1/4*(Psi(1/2+c2*I/4)+Psi(1/2-c2*I/4)-Psi(1+c2*I/4)
          -Psi(1-c2*I/4)):

 K[i,j]:=evalf(2*h/Pi*(J1+J2)/(2*L));
 # we know that K doesn't have imaginary part.

end do:
end do:

II:=IdentityMatrix(N):

A:=II-K: # A*Phi=B, A is the coefficient Matrix

B:=Matrix(N,1):

for i from 1 to N do
```

```
    B[i,1]:=2/Pi:
end do:

phi:=LinearSolve(A,B):   # function phi

# here we assume that phi is piecewise constant in each segments

w:=0:
 for i from 1 to N do
    w:=w+phi[i,1]:
end do:

g:=h*w:  # g is the integral of phi over x from 0 to 1

I_R1:=evalf(2*Pi*g)*a *Omega;
# I_R1 is the current passing through the spot
```

```
# Solving the Fredholm integral equation by the rectangular rule
  (Type II)

with(LinearAlgebra):

L:=2:   # L is the dimensionless thickness
n:=20:  # n is the number of points. The fist point is x(1).
N:=n-1: # N is the number of intervals
h:=1/N: # h is the length of each interval

# x is the vector of the points between 0 and 1

for i from 1 to N do  # x(i) starts from x(1)=h to x(N)=1
  x(i):=h*i:
end do:

K:=Matrix(n-1):  # K matrix is the matrix of the kernel integral

for i from 1 to N do
 for j from 1 to N do

c1:=(x(i)+x(j))/L:
c2:=(x(i)-x(j))/L:
J1:=-1/4*(Psi(1/2+c1*I/4)+Psi(1/2-c1*I/4)-Psi(1+c1*I/4)
          -Psi(1-c1*I/4)):
J2:=-1/4*(Psi(1/2+c2*I/4)+Psi(1/2-c2*I/4)-Psi(1+c2*I/4)
          -Psi(1-c2*I/4)):
```

```
 K[i,j]:=evalf(2*h/Pi*(J1+J2)/(2*L));
# we know that K doesn't have imaginary part.

end do:
end do:

II:=IdentityMatrix(N):
A:=II-K: # A*Phi=B, A is the coefficient Matrix
B:=Matrix(N,1):

for i from 1 to N do
    B[i,1]:=2/Pi:
end do:

phi:=LinearSolve(A,B):   # function phi

# here we assume that phi is piecewise constant in each segments

w:=0:
 for i from 1 to N do
    w:=w+phi[i,1]:
end do:
g:=h*w:  # g is the integral of phi over x from 0 to 1

I_R2:=evalf(2*Pi*g)*a *Omega;
# I_R2 is the current passing through the spot
```

```
# Solving the Fredholm integral equation by trapezoidal rule

with(LinearAlgebra):
L:=2:   # L is the dimensionless thickness
n:=21:  # n is the number of points. The fist point is x(1).
N:=n-1: # N is the number of intervals
h:=1/N: # h is the length of each interval

# x is the vector of the points between 0 and 1
for i from 1 to n do  # x(i) starts from x(1)=0 to x(n)=1
  x(i):=h*(i-1):
end do:

K:=Matrix(n):   # K matrix is the matrix of the kernel integral

for i from 1 to n do
 for j from 1 to n do

c1:=(x(i)+x(j))/L:
c2:=(x(i)-x(j))/L:

J1:=-1/4*(Psi(1/2+c1*I/4)+Psi(1/2-c1*I/4)-Psi(1+c1*I/4)
          -Psi(1-c1*I/4)):
J2:=-1/4*(Psi(1/2+c2*I/4)+Psi(1/2-c2*I/4)-Psi(1+c2*I/4)
          -Psi(1-c2*I/4)):

 K[i,j]:=evalf(2/Pi*(J1+J2)/(2*L)):
```

```
 # we know that K doesn't have imaginary part.

end do:
end do:

# The following is to consider the trapezoidal rule
for i from 1 to n do
  K[i,1]:=1/2*K[i,1]:
  K[i,n]:=1/2*K[i,n]:
end do:


A:=Matrix(n,1):
for i from 1 to n do
    A[i,1]:=2/Pi:
end do:

II:=IdentityMatrix(n):

T:=II-h*K:  # T*Phi=A, T is coefficient Matrix

phi:=LinearSolve(T,A): # function phi

# we assume that phi is linear in each interval

w:=0:  # Trapezoidal Rule
for i from 1 to n do
```

```
  w:=w+h*phi[i,1]:
end do:

ww:=w-h/2*(phi[1,1]+phi[n,1]):

I_T:=evalf(2*Pi*ww)*a *Omega;
#I_T is the current passing through the spot
```

```
# Solving the Fredholm integral equation by Simpson's rule

with(LinearAlgebra):
L:=2:   # L is the dimensionless thickness
n:=21:  # n is the number of points. The fist point is x(1).
N:=n-1: # N is the number of intervals
h:=1/N: # h is the length of each interval

# x is the points between 0 and 1
for i from 1 to n do  # x(i) starts from x(1)=0 to x(n)=1
  x(i):=h*(i-1):
end do:

K:=Matrix(n):   # K matrix is the matrix of the kernel integral

for i from 1 to n do
 for j from 1 to n do

c1:=(x(i)+x(j))/L:
c2:=(x(i)-x(j))/L:

J1:=-1/4*(Psi(1/2+c1*I/4)+Psi(1/2-c1*I/4)-Psi(1+c1*I/4)
          -Psi(1-c1*I/4)):
J2:=-1/4*(Psi(1/2+c2*I/4)+Psi(1/2-c2*I/4)-Psi(1+c2*I/4)
          -Psi(1-c2*I/4)):

 K[i,j]:=evalf(2/Pi*(J1+J2)/(2*L)):
```

```
 # we know that K doesn't have imaginary part.

end do:
end do:

DD:=Matrix(n,1):
# DD is the coefficient matrix for Simpson's rule
for i from 2 by 2 to n-1 do
    DD[i,1]:=4*h/3:
end do:

for i from 3 by 2 to n-2 do
    DD[i,1]:=2*h/3:
end do:

DD[1,1]:=h/3:
DD[n,1]:=h/3:

M:=Matrix(n):
# M is a n*n matrix which its diagonal arrays are the same as
  A matrix arrays and the other arrays of M are zero.

for i from 1 to n do
  M[i,i]:=DD[i,1]:
end do:

II:=IdentityMatrix(n):
```

```
T:=II-K.M:
# T*Phi=A, T is the coefficient Matrix.

# A Matrix is defined as:
A:=Matrix(n,1):
for ii from 1 to n do
    A[ii,1]:=2/Pi:
end do:

phi:=LinearSolve(T,A): # function phi


# we assume that phi is parabolic in each interval

z:=0:   # Simpson's Rule (n must be odd)
 for i from 2 by 2 to n-1 do
   z:=z+4*h/3*phi[i,1]:
end do:
for i from 3 by 2 to n-2 do
    z:=z+2*h/3*phi[i,1]:
end do:
zz:=z+h/3*(phi[1,1]+phi[n,1]):
I_S:=evalf(2*Pi*zz)*a *Omega;
#I_S is the current passing through the spot
```

Bibliography

[1] L. Kogut and K. Komvopoulos. Electrical contact resistance theory for conductive rough surfaces. *Journal of Applied Physics* 94(5), September 1 2003.

[2] Jack W. Judy. Microelectromechanical Systems (MEMS): Fabrication, Design, and Application. *Journal of Smart Materials and Structures*, 10:115-1134, 2001.

[3] J. Jason Yao. TOPICAL REVIEW: RF MEMS from a device perspective. *Journal of Micromechanics and microengineering*, 10(4):R9-R38, 2000.

[4] S. E. Lyshevski. MEMS and NEMS: systems, devices, and structures. *CRC Press, USA*, 2001.

[5] Ye Wang et al. A micromachined RF microreley with electrothermal actuation. *Journal of Sensors and Actuators A*, 103:231-236, 2003.

[6] G.M. Rebeiz and J.B. Muldavin. RF MEMS switches and switch circiuts. *IEEE microwave magazine*, December 2001.

[7] G.M. Rebeiz. RF MEMS Theory, Design, and Technology. *Wiley Interscience*, 2003. New Jersey.

[8] B.D. Jensen, L.L.Chow, K. Huang, K. Saitou, J.L. Volakis, and K. Kurabayashi. Effect of Nanosclae Heating on Electrical Transport in RF MEMS Switch Contacts. *Journal of Microelectromechanical Systems*, 14(5):935-946, October 2005.

[9] S. Majumder, N.E. McGruer, G.G. Adams, P.M. Zavracky, R.H. Morrison, and J. Krim. Study of contacts in an electrostatically actuated microswitch. *Sens. Actuators A: Phys.*, 93:19-26, 2001.

[10] R. Holm. Electric Contacts, Theory and Application. *Springer, 4th edition, New York*, 1967.

[11] F.P. Bowden and J.B.P. Williamson. Electrical conduction in solids, I. Influence of the Passage of Current on the Contact between Solids. *Proceedings of Royal Society of London A*, 246(1244):1-12, July 1958.

[12] Seik Oh and Michael D. Bryant. The Transient Temperature Fields for Two Contacting Bodies Having Different Electrical Potentials. *IEEE Transactions on Components, Hybrids, and Manufacturing Technology*, 9(1):71-76, March 1986.

[13] J.A. Greenwood and J.B.P. Williamson. Electrical conduction in solids, II. Theory of temperature-dependent conductors. *Proceedings of Royal Society of London A*, 246(1244):13-31, July 1958.

[14] Jiang Zhu. Interfacial Temperatures at MEMS Switch Contact Asperities. *Master's dissertation, The University of Western Ontario*, 2006.

[15] A.F. Mills. Heat Transfer. *second edition, Prentice Hall, Inc.*, 1999.

[16] N.H. Frank. Introduction to Electricity and Optics. *second edition, Mcgraw-Hill Book Company, Inc.*, 1950.

[17] H.S. Carslaw and J.C. Jaeger. Conduction of Heat in Solids. *Oxford University Press*, 1959.

[18] A.P. Prudnikov, Yu.A. Brychkov, and O.I. Marichev. Integrals and Series, *Gordon and Breach Science Publishers, Philadelphia, Pennsylvania, USA*, 1992.

[19] Francis B. Hildebrand. Methods of Applied Mathematics. *second edition, Dover Publications, Inc.*, 1992.

[20] Ian N. Sneddon. Mixed boundary value problems in potential theory. *John Wiley & sons, Inc.*, 1966.

[21] C. J. Tranter. On some dual integral equations occuring in potential problems with axial symmetry. *Quarterly Journal of Mechanics and Applied Mathematics*, 3(4): 411-419, 1950.

[22] Fuqian Yang. Solution of a dual integral equation for crack and indentation problems. *Theoritical and Applied Fracture Mechanics*, 26(3): 211-217, 1997.

[23] Paul G. Slade. Electrical Contacts: Principles And Applications. *Marcel Dekker, Inc.*, 1999.

[24] Milenko Braunovic. Electrical Contacts: Fundamentals, Applications and Technology. *CRC Press*, 2007.

[25] Robert Weinstock. Calculus of Variations. *Dover Publications, Inc.*, 1974.

[26] Gradshteyn and Ryzhik. Table of Integrals, Series, and Products. *Academic Press, Inc.*, 1994.

[27] F. G. Tricomi. Integral Equations. *Dover Publications, Inc.*, 1957.

[28] S. D. Conte. Elementary Numerical Analysis. *McGraw-Hill Book, Inc.*, 1965.